

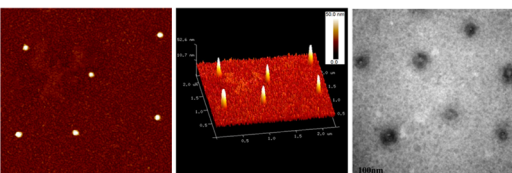
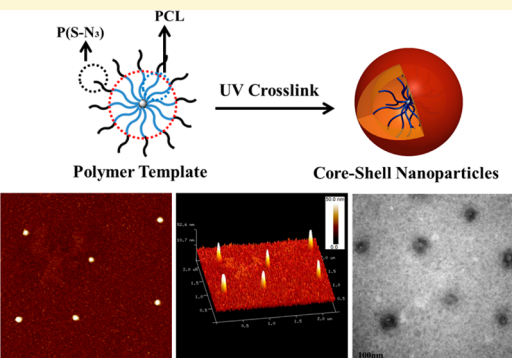
# Robust Route to Unimolecular Core–Shell and Hollow Polymer Nanoparticles

Chaowei Feng, Xinchang Pang, Yanjie He, Bo Li, and Zhiqun Lin\*

School of Materials Science and Engineering, Georgia Institute of Technology, Atlanta, Georgia 30332, United States

Supporting Information

**ABSTRACT:** Unimolecular core–shell and hollow polymer nanoparticles with well-defined dimensions were crafted using spherical core–shell star-like diblock copolymers as templates. Monodisperse and structurally stable star-like diblock copolymers composed of inner degradable core blocks and outer photo-cross-linkable shell blocks were synthesized via a combination of two living polymerization techniques, namely, coordination–insertion ring opening polymerization (ROP) followed by reversible addition–fragmentation chain-transfer polymerization (RAFT). Subsequently, uniform unimolecular core–shell nanoparticles were successfully produced by photo-cross-linking the shell blocks of star-like diblock copolymers. The core diameter and shell thickness of nanoparticles are determined by molecular weights of inner core block and outer shell block, respectively, thereby rendering nanoparticles with tunable structural characteristics. The cross-linking density of nanoparticles can be readily controlled by varying the exposure time of star-like diblock copolymer templates to UV illumination. The selective degradation of inner core blocks yielded hollow polymer nanoparticles which retained structural integrity. The dye encapsulation and release studies revealed that unimolecular core–shell nanoparticles may be exploited as a new class of nanocarriers and promising drug nanovehicles.



## INTRODUCTION

Amphiphilic linear block copolymers possess the propensity to self-assemble into a large variety of complex nanoscale assemblies, including spherical micelles,<sup>1</sup> cylindrical or worm-like micelles,<sup>2</sup> and vesicles,<sup>3</sup> when dispersed in selective solvents.<sup>4</sup> These nanoscale micelles are, however, often kinetically trapped in nonequilibrium states. As a result, their characteristics and shapes for a given system depend sensitively on concentration, solvent properties, temperature, and pH, etc.,<sup>5</sup> and are subject to vary in response to changes in these experimental conditions.<sup>6</sup> For example, dissociation of nanoscale assemblies into individual linear polymer chains can occur when the solution concentration decreases below the critical micelle concentration (CMC). Thus, cross-linking of either the core or shell of self-assembled nanostructures is carried out to improve their stability by essentially locking in the structures.<sup>7–9</sup> However, the access to core–shell polymer nanoparticles that are dimensionally and functionally well-defined is still limited due in part to the relatively poor size control and comparatively high polydispersity of nanostructures obtained via self-assembly of linear block copolymers.<sup>10,11</sup> It is noteworthy that the common need for amphiphilic characteristics of block copolymers in order to impart self-assembly restricts the scope of selection on their chemical compositions and functionalities. Clearly, it is challenging to realize well-tailored core–shell or hollow polymer nanoparticles from self-assembled micelles.

In stark contrast to micelles comprising linear amphiphilic polymer chains that are dynamically stable as noted above, star-like polymers can readily form static unimolecular micelles in solution, that is, structurally stable spherical macromolecules. Star-like polymers are a class of branched macromolecules in which multiple linear chains or arms are covalently connected to a multifunctional core. A variety of star-shaped homopolymers and core–shell block copolymers as well as miktoarm star polymers have been synthesized by living polymerization techniques via either the core-first or arm-first approach.<sup>12–16</sup> Recent advances in living/controlled polymerization render the preparation of star-like core–shell block copolymers with a precisely controllable topology. Intriguingly, they may be utilized as unimolecular micellar templates for creating core–shell and hollow polymer nanoparticles with controlled dimensions and compositions. This has yet to be explored.

Drug delivery and controlled release technologies have made a pronounced impact on the medical field.<sup>17</sup> Loading guest chemotherapeutic agents in nanocarriers can result in improved drug stability, reduced clearance, and long circulation time. In this context, a variety of nanocarriers have been developed for drug delivery applications, including liposome, polymer–drug conjugates,<sup>18</sup> polymer micelle nanoparticles,<sup>19,20</sup> and unimolecular micelles.<sup>21,22</sup> Among them, polymer micelle nano-

Received: August 23, 2014

Revised: September 27, 2014

Published: September 29, 2014

particles<sup>23</sup> have received attention due to highly enhanced drug solubility and long circulating half-life. Unimolecular micelles exhibit improved stability compared to self-assembled polymer micelles. However, they are still unstable above the critical aggregation concentration (CAC) and the aggregation is often observed.<sup>24–26</sup> It is worth noting that the instability would trigger premature drug release and potentially harm healthy tissue.<sup>21,24</sup> A well-controlled size is particularly important for tumor-targeted drug delivery as the effective size of nanocarriers falls in the range of 20–100 nm.<sup>27,28</sup> In this context, it is highly desirable yet challenging to create structurally well-defined nanostructures with good stability, monodispersity, and precise size controllability as a new type of drug vehicle.

Herein, we report a robust strategy for crafting monodisperse unimolecular core–shell and hollow nanoparticles by exploiting star-like core–shell diblock copolymers comprising biodegradable inner blocks (i.e., core blocks) and photo-cross-linkable outer blocks (i.e., shell blocks containing photo-cross-linkable azido functionalities) as templates. Star-like photo-cross-linkable core–shell diblock copolymers were synthesized by a combination of two consecutive living polymerization techniques, and adopted a spherical conformation. Photo-cross-linking of azido moieties in the shell blocks was chosen to yield uniform unimolecular core–shell nanoparticles as the photo-cross-linking proceeds under simple and mild UV irradiation and the cross-linking density can be facilely tuned by varying UV intensity and irradiation time.<sup>29,30</sup> By selectively removing the core blocks, hollow polymer nanoparticles can be formed, suggesting the *in vitro* degradability of inner blocks. The versatility of unimolecular core–shell nanoparticles as intriguing and effective nanocarriers for potential use as drug nanovehicles was elaborated by loading dyes (e.g., rhodamine B) as model compounds in nanoparticles. Dye-loaded nanoparticles with controlled size and low polydispersity were obtained as a result of spherical shape and monodisperse characteristics of star-like core–shell diblock copolymer templates. More importantly, the release behavior of dyes within nanocarriers was tracked by fluorescence spectroscopy. It is interesting to note that the dimension of nanoparticles, that is, the diameter of the core and the thickness of the shell, can be readily controlled by simply tuning the molecular weights of the core block and the photo-cross-linkable shell block, respectively. These rationally designed photo-cross-linkable core–shell star-like diblock copolymers hold promise for the construction of unimolecular polymer nanoparticles as nanocarriers and delivery vehicles.

## ■ EXPERIMENTAL SECTION

**Materials.** Stannous octoate ( $\text{Sn}(\text{Oct})_2$ , 95%), oxalyl chloride ( $\geq 99\%$ ), 2-(dodecylthiocarbonothioylthio)-2-methylpropionic acid (TC, 98%, HPLC grade), Rhodamine B (RhB, 95%), sodium azide ( $\geq 99.5\%$ ), and anhydrous  $\text{MgSO}_4$  were purchased from Sigma-Aldrich and used as received.  $\beta$ -cyclodextrin ( $\beta$ -CD, Sigma-Aldrich) was dried at 80 °C under reduced pressure overnight prior to use.  $\epsilon$ -Caprolactone ( $\epsilon$ -CL, Sigma-Aldrich, 97%) and 4-chloromethylstyrene (Sigma-Aldrich, 90%) were distilled over  $\text{CaH}_2$  under reduced pressure prior to use. Ruthenium (VIII) oxide (Strem Chemicals Inc, 0.5%) was used as received. Anhydrous dichloromethane (DCM) and *N,N*-dimethylformamide (DMF) were obtained from a commercial solvent purification system (MB-SPS, MBraun Inc.). Osmapentalyne was obtained from Xiamen University, China.<sup>31</sup> All other reagents were purified by common purification procedures.

**Synthesis of Star-Like PCL.** Twenty-one-arm star-like polycaprolactone (PCL) was synthesized via controlled ring opening

polymerization of  $\epsilon$ -CL using  $\beta$ -CD as multifunctional initiator and  $\text{Sn}(\text{Oct})_2$  as catalyst. To impart efficient initiation and homogeneous polymerization, DMF was used as solvent to solubilize  $\beta$ -CD. All polymerizations were performed under stringent anhydrous conditions to avoid initiation from water. Three samples with different molecular weights were synthesized by varying the  $\text{Sn}(\text{Oct})_2$  concentration or temperature (Supporting Information (SI) Table S1). It is clear that larger catalyst concentration and higher temperature resulted in faster polymerization rate and nearly complete monomer conversion (SI Table S1). As demonstrated elsewhere,<sup>32,33</sup> ring opening polymerization catalyzed by  $\text{Sn}(\text{Oct})_2$  proceeds with *in situ* metal alkoxide generated as the active center, and it is the fast dynamic exchange between dormant and reactive species that maintains living polymerization characteristics. Thus, the polymerization rate increased as a result of increased concentration of reactive center in an equilibrium with dormant  $-\text{OH}$  species at the  $[\text{Sn}]/[\text{OH}]$  ratio below 0.5. On the other hand, the increase in temperature led to faster reaction rate due to higher rate constant.

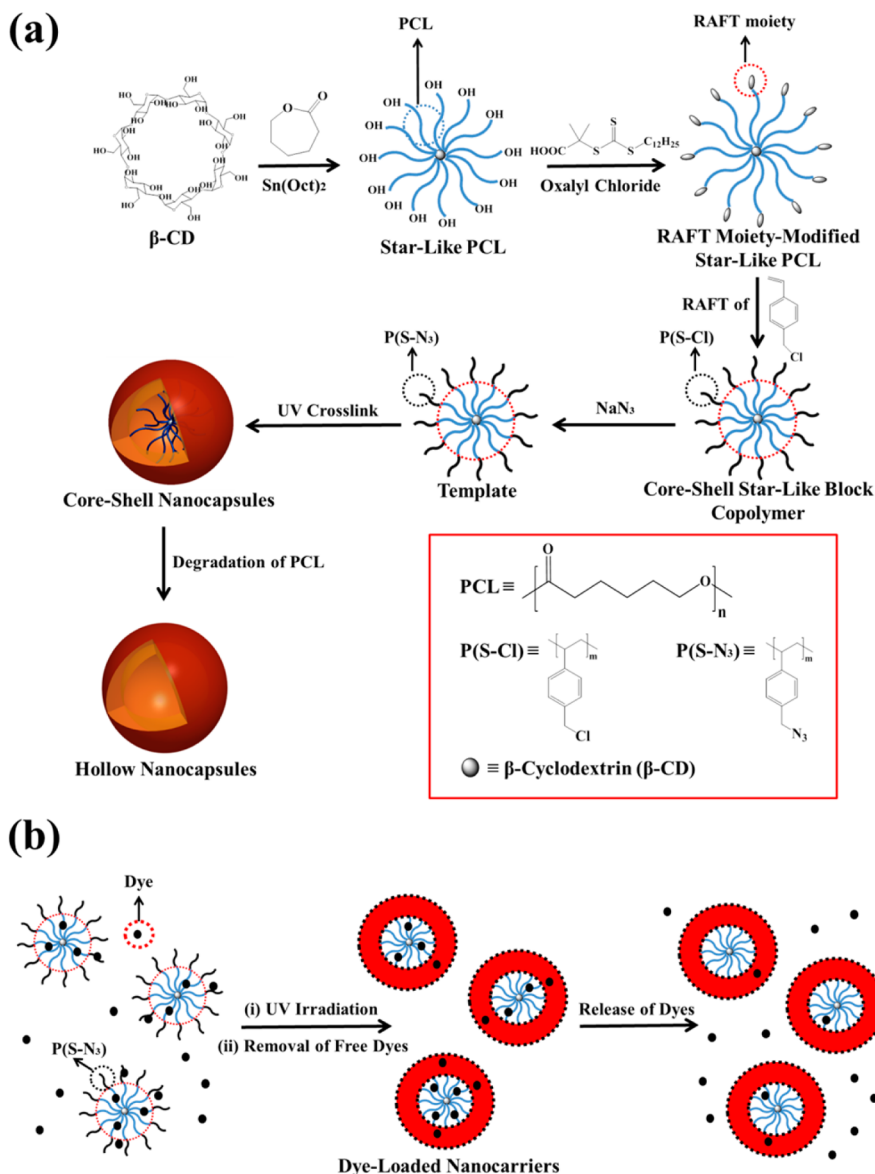
A typical polymerization procedure is described as follows: A flame-dried ampule was connected to a Schlenk-line where the exhausting–refilling processes were repeated for three times.  $\beta$ -CD (97.5 mg) was dried at 80 °C under reduced pressure overnight, which was subsequently dissolved in anhydrous DMF and transferred into a reaction ampule together with  $\text{Sn}(\text{Oct})_2$  (36.5 mg) and dry  $\epsilon$ -CL monomer (10 mL) under argon atmosphere. The ampule was then immersed into an oil bath at 130 °C. The polymerization was allowed to proceed for a desirable amount of time. After being cooled to room temperature, the crude polymer was diluted with chloroform and precipitated in cold methanol for three times, yielding the purified product. The pure homopolymer was finally dried in vacuum oven. Yield: 10 g (97.1%).

**Synthesis of TC-End-Functionalized Star-Like PCL (i.e., PCL-TC).** A round-bottom flask was connected to a Schlenk line where exhausting–refilling processes were repeated for three times. Tri thiocarbonate RAFT agent (TC; 0.12g) was dissolved in anhydrous  $\text{CH}_2\text{Cl}_2$  (5 mL) and then transferred to a flask under argon atmosphere, followed by the addition of oxalyl chloride (0.43 mL). The reaction mixture was stirred at room temperature for 3 h until the gas evolution stopped. The excess reagents were then removed via rotary evaporation. The residue was redissolved in anhydrous  $\text{CH}_2\text{Cl}_2$  (5 mL). Subsequently, star-like PCL solution (1 g in 15 mL of  $\text{CH}_2\text{Cl}_2$ ) was added. After stirring at room temperature for 19 h, the content was precipitated in cold methanol for three times. The product was finally dried at 50 °C in a vacuum oven. Yield: 0.92 g (90%).  $^1\text{H}$  NMR: Conversion >95%.

**Synthesis of Core–Shell Star-Like PCL-b-(P(S–Cl)) via RAFT.** Core–shell star-like polycaprolactone-block-poly(4-chloromethylstyrene) (denoted PCL-b-P(S–Cl)) was effectively prepared by reversible addition–fragmentation polymerization (RAFT) of 4-chloromethylstyrene in toluene in the presence of star-like PCL-TC as the mediating chain transfer agent via thermal initiation. In a typical process, an ampule charged with star-like PCL-TC (0.15g), 4-chloromethylstyrene monomer (1.67 mL), and toluene (4.28 mL) was degassed by three freeze–evacuate–thaw cycles in liquid  $\text{N}_2$ , and then sealed. The polymerization was conducted at 120 °C without adding azobis(isobutyronitrile) (AIBN) initiator. After proceeding to a desirable time, the reaction was quenched by immersion in liquid  $\text{N}_2$ . The reaction mixture was then diluted with  $\text{CH}_2\text{Cl}_2$  and precipitated in cold methanol to obtain crude product. To remove linear homopolymer produced during the RAFT process, the selective precipitation of crude product in a tetrahydrofuran (THF)/methanol mixture was performed three times to yield pure copolymers. The final product was dried to a constant weight under vacuum at 50 °C.

**Synthesis of Cross-Linkable Copolymer Template Star-Like PCL-b-P(S–N<sub>3</sub>).** The chlorine groups on P(S–Cl) shell blocks in PCL-b-P(S–Cl) were substituted by azido functionalities to produce star-like PCL-b-P(S–N<sub>3</sub>) template. Specifically, star-like PCL-b-P(S–Cl) (50 mg) and sodium azide (55 mg) were mixed in DMF (4 mL). The reaction mixture was stirred at room temperature for 24 h, and then precipitated in cold methanol. The crude product was redissolved

**Scheme 1.** (a) Synthetic Strategy for Unimolecular Polymeric Core–Shell and Hollow Nanocapsules and (b) Encapsulation and Release of Dyes



in  $\text{CH}_2\text{Cl}_2$ , and then washed with distilled water three times. The obtained organic layer was dried by anhydrous  $\text{MgSO}_4$ , and precipitated in cold methanol again after concentration. The final pure product was collected and then dried in vacuum oven at  $40^\circ\text{C}$ .

**Preparation of Unimolecular Core–Shell Polymer Nanoparticles via Intramolecular Cross-Linking.** Core–shell polymeric nanoparticles were formed by cross-linking pendant azido groups on the shell blocks of the star-like copolymer template via UV irradiation ( $\lambda = 254$  nm, power = 4 W, intensity = 0.76 mW/cm<sup>2</sup> at 3 in.). It is worth noting that the dilute condition was invoked to ensure only intramolecular cross-linking. In a typical procedure, star-like PCL-*b*-P(S-N<sub>3</sub>) template (2 mg) was dissolved in chloroform (4 mL) and filtered using a 0.45-μm PTFE filter. The solution was then exposed to UV irradiation at room temperature under stirring in a quartz container. The cross-linking was stopped at various exposure times to afford different degrees of cross-linking density. The mixture was then concentrated under vacuum and precipitated in methanol to yield final product.

**Formation of Hollow Nanoparticles by Degrading Core Blocks.** Core–shell nanoparticles (7 mg) were dissolved in 22 mL of dioxane with the addition of 1 mL of 10 M HCl solution. The reaction mixture was placed in a constant temperature oil bath at  $90^\circ\text{C}$  and

refluxed for 3 days. The solution was then concentrated and precipitated in methanol to yield final product.

**Encapsulation of Dyes.** Because of the intrinsic spherical shape of star-like PCL-*b*-P(S-N<sub>3</sub>) diblock copolymer and the stable characteristics of cross-linked core–shell nanoparticles, a simple yet versatile encapsulation technique using dye as a model compound was developed. Briefly, star-like diblock copolymer templates (1 mg) were mixed with dyes (RhB (14 mg) or osmapentalyne (10 mg)) in  $\text{CHCl}_3$  (2 mL). The solution was filtered using a 0.45-μm PTFE filter. The mixture was then exposed to UV irradiation for various exposure times under stirring at room temperature to form dye-loaded nanoparticles. The organic solvent was removed or concentrated under reduced pressure. To remove dyes that were not encapsulated within nanoparticles, nanoparticles were washed with methanol for a desirable amount of time and separated via centrifugation at 5000 rpm for 5 min. Final products (i.e., nanocarriers) were found to exhibit the same color as dyes.

**Dye Release Study.** For the dye release studies, RhB-loaded nanoparticles were redispersed in solvent (chloroform or THF). Subsequently, fluorescence emission spectra of solution were directly measured at predetermined times. The amount of RhB released from

**Table 1.** Structural Parameters of Polymer Precursors and the Prepared Nanoparticles

		$M_{n,NMR}^a$ (kg/mol)	$M_{n,GPC}^b$ (kg/mol)	$M_{n,theory}^c$ (kg/mol)	core $N^d$	shell $N^d$	core size, $D_{core}^e$ (nm)	overall size, $D_{overall}^e$ (nm)	PDI <sup>f</sup>
star PCL- <i>b</i> -(P(S-Cl))	(sample a)	183.5	109.6	174.1	53	15			1.10
	(sample b)	194.4	115.6	221.7	53	19			1.12
	(sample c)	236.1	146.7	277.2	53	32			1.14
star PCL- <i>b</i> -(P(S-N <sub>3</sub> )) nanoparticles	(template)	240.5	142.0	281.6	53	32	34.6	63.7	1.14
							25.1	58.4	0.11

<sup>a</sup>Molecular weights calculated from NMR analysis based on molecular weights of precursors (i.e., PCL-TC). <sup>b</sup>Molecular weights determined by GPC using PS as the calibration standard. <sup>c</sup>Theoretical molecular weights calculated based on the monomer to initiator feeding ratio and conversion.

<sup>d</sup>Number of repeating units obtained by NMR analysis. <sup>e</sup>Sizes obtained from DLS for star-like diblock copolymer template (i.e., the intensity hydrodynamic diameter  $D_h$  of star-like PCL for  $D_{core}$ , and the intensity hydrodynamic diameter  $D_h$  of star PCL-*b*-P(S-N<sub>3</sub>) for  $D_{overall}$  (Sample 3 in SI Table S1)), and from TEM image analysis for nanoparticles. <sup>f</sup>Polydispersity obtained from GPC for polymers (i.e., samples a–c and template) and DLS for nanoparticles, respectively. Note: all nanoparticles were produced using template derived from sample c.

nanoparticles into solution was tracked by monitoring the fluorescence intensity at the emission wavelength of 572 nm (excited at 559 nm).

**Characterizations.** Molecular weights of polymers were obtained by gel permeation chromatography (GPC, Shimadzu) equipped with a LC-20AD HPLC pump and a refractive index detector (RID-10A, 120 V). THF was used as the mobile phase at the flow rate of 1.0 mL/min at 35 °C. One Phenogel 5 μm linear column and one Phenogel 5 μm 10E4A mixed bed column were calibrated with 10 polystyrene standard samples with molecular weights ranging from  $1.2 \times 10^6$  to 500 g/mol. All <sup>1</sup>H nuclear magnetic resonance (NMR) spectra were obtained using a Bruker 400 MHz spectrometer with the solvent resonances as the internal standard. CDCl<sub>3</sub> was used as the solvent in all measurements. The morphologies of core–shell and hollow nanoparticles were examined by atomic force microscope (AFM, Bruker Dimension Icon; operated in the tapping mode at 0.5 Hz scanning rate). The samples for AFM measurements were prepared by spin-coating the dilute nanocapsule solution onto Si substrate at 3000 rpm for 1 min (Headway PWM32 spin coater). Core–shell and hollow nanoparticles were also imaged by transmission electron microscopy (TEM) (JEOL TEM 100CX; operated at 100kv). TEM samples were prepared by drop-coating a dilute nanocapsule solution onto the 400 mesh carbon-coated copper TEM grid. Prior to TEM imaging, samples were subsequently stained with RuO<sub>4</sub> vapor for various times. Dynamic light scattering (DLS) measurements were performed using a laser light scattering spectrometer (Malvern Zetasizer Nano ZS) at 25 °C. A DAWN-EOS light scattering instrument (Wyatt Technology) equipped with a GaAs laser ( $\lambda_0 = 685$  nm) as the light source and a K5 flow cell was used for static light scattering (SLS) measurements. FTIR spectra were collected on the Shimadzu IRAffinity1 spectrometer equipped with a Miracle Single Reflection Horizontal ATR Accessory (Pike Technologies). UV-visible spectra were recorded using a Shimadzu UV-2600 UV-vis spectrophotometer. The photoluminescence spectra were taken using a Shimadzu RF-5301 spectrofluorometer (equipped with a 150 W xenon lamp light source and a R928 photomultiplier), covering a wavelength range of 220–900 nm with a resolution of 1.5 nm.

## RESULTS AND DISCUSSION

**Synthesis of Core–Shell Star-Like Diblock Copolymers.** The synthetic route to unimolecular polymer nanoparticles based on core–shell star-like block copolymers is depicted in Scheme 1a. The core-first approach was employed to yield high initiation efficiency and a well-defined architecture of the resulting star-like block copolymers. Because of the hydrolytic and in vivo degradability of poly( $\epsilon$ -caprolactone) (PCL), star-like PCL with terminal hydroxyl functionalities was synthesized as the biodegradable core. Specifically, star-like PCL with narrow molecular weight distribution (i.e., polydispersity index, PDI < 1.1) was synthesized via coordination–insertion ring opening polymerization (ROP)

of  $\epsilon$ -caprolactone by using Sn(Oct)<sub>2</sub> as catalyst and  $\beta$ -cyclodextrin ( $\beta$ -CD) with 21 hydroxyl groups on its surface as initiator due to its biocompatibility (Scheme 1a). Three samples with different molecular weights were synthesized and results are summarized in SI Table S1. The methylene proton signal at 3.64 ppm in <sup>1</sup>H NMR spectrum indicated that star-like PCL was terminated by hydroxyl end groups (SI Figure S1a). The molecular weights were calculated based on the integration ratio of H<sup>e</sup> to H<sup>f</sup> (I<sup>e</sup>/I<sup>f</sup>) (SI Figure S1a), assuming that each hydroxyl group on  $\beta$ -CD participated in the initiation. The consistency between  $M_{n,th}$  and  $M_{n,NMR}$  suggested that the initiation efficiency for polymerization of  $\epsilon$ -caprolactone was nearly quantitative, leading to the formation of star-like PCL with 21 arms. In addition, GPC traces displayed monomodal distribution in all samples (SI Figure S2a).

RAFT was selected to graft the second block poly(4-chloromethylstyrene) (P(S-Cl)) due to its high versatility and compatibility with 4-(chloromethyl)styrene monomer.<sup>34,35</sup> First, trithiocarbonate (TC)<sup>36</sup> was grafted onto star-like PCL (i.e., sample 3 in SI Table S1) by coupling with its end hydroxyl groups to form R-connected<sup>37</sup> polymeric RAFT agent (i.e., PCL-TC). The success in grafting was confirmed by NMR (SI Figure S1b) and UV–vis spectroscopy measurements (a characteristic absorption peak of TC is at 308 nm, SI Figure S3). Subsequent chain extension from star-like PCL-TC by RAFT polymerization of 4-(chloromethyl)styrene was performed to yield star-like PCL-*b*-P(S-Cl) diblock copolymer with P(S-Cl) as shell. In the synthesis of star polymers by RAFT using the R-group approach,<sup>37</sup> high radical flux and long reaction time would easily result in excess star–star coupling termination for slowly propagating monomers such as styrene and its derivatives.<sup>37</sup> Thus, thermal initiation was utilized in the chain extension step to avoid undesirable star–star coupling. Any additional initiator would lead to multimodal molecular weight distribution due to high radical flux, and thus excess termination reactions in the system. We note that linear polymers including linear macro-RAFT agent and terminated chains may be inevitably generated during polymerization, as evidenced by the tail present in low molecular weight region in GPC traces (SI Figure S2b)<sup>37</sup> and were removed prior to further reaction in order to obtain pure star-like PCL-*b*-P(S-Cl) diblock copolymers (SI Figure S2c). We note that samples a–c (i.e., star-like PCL-*b*-P(S-Cl); Table 1) were prepared by grafting P(S-Cl) from sample 3 (i.e., star-like PCL; SI Table S1), and only sample c was subsequently used to produce core–shell and hollow polymer nanoparticles described in the

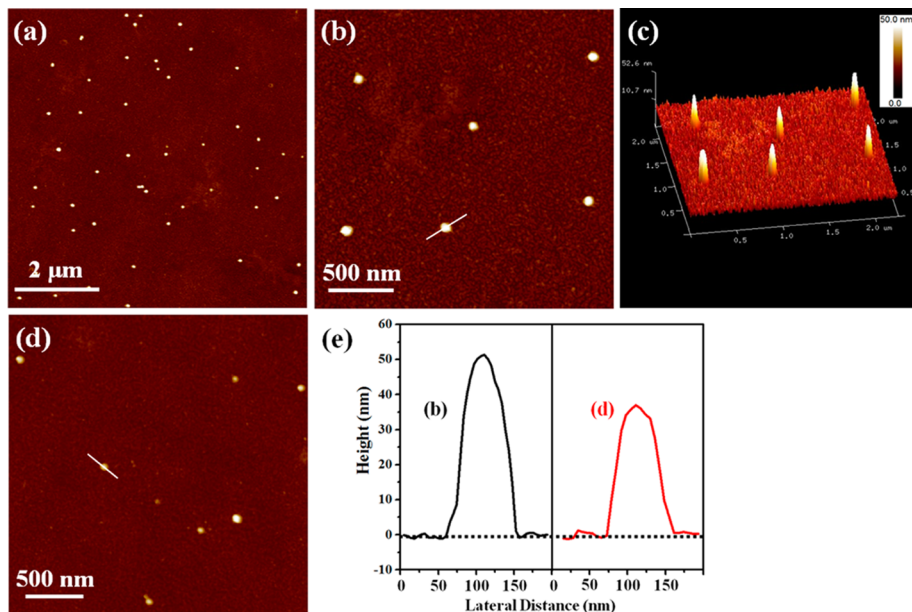


**Figure 1.** Core–shell nanoparticles obtained from cross-linking of star-like PCL-*b*-P(S–N<sub>3</sub>) template in Table 1. (a) AFM height image of uniform fully cross-linked nanoparticles after exposure to UV irradiation for 70 min. (c) Representative 3D height image of fully cross-linked nanoparticles. (b) and (d) AFM height images of fully cross-linked and partially cross-linked (after a 20 min UV exposure) nanoparticles, respectively. (e) Cross-sectional profiles of fully cross-linked and partially cross-linked nanoparticles obtained from the corresponding AFM height images in (b) and (d), respectively (i.e., straight lines across nanoparticles in (b) and (d)).

following two sections. The pendant chlorides on the shell block were then substituted by azido groups to introduce photo-cross-linkable moieties (i.e., N<sub>3</sub> groups) and yield photo-cross-linkable star-like PCL-*b*-P(S–N<sub>3</sub>) diblock copolymer (Table 1). Complete shift of –CH<sub>2</sub>– adjacent to –N<sub>3</sub> upfield to new position at 4.27 ppm in <sup>1</sup>H NMR spectra was indicative of a nearly complete conversion of benzyl chlorides (SI Figure S4). <sup>1</sup>H NMR spectra (SI Figures S1 and S4) and GPC traces (SI Figure S2) of intermediate and final products after each transformation step suggested the successful synthesis of well-defined core–shell star-like diblock copolymer with low polydispersity as summarized in Table 1. The molecular weights of polymers derived from <sup>1</sup>H NMR are different from those obtained by GPC due to their different hydrodynamic volumes in comparison to linear PS standards. The molecular weight of each block in star-like diblock copolymers can be readily controlled by living polymerization techniques (i.e., ROP and RAFT), which is of key importance in yielding uniform sizes of both core and shell blocks for producing monodisperse polymeric nanoparticles. It is also noteworthy that the grafting-from strategy employed in the present study enabled the crafting of diblock copolymers with well-tailored star-like architectures and high grafting density of arms.

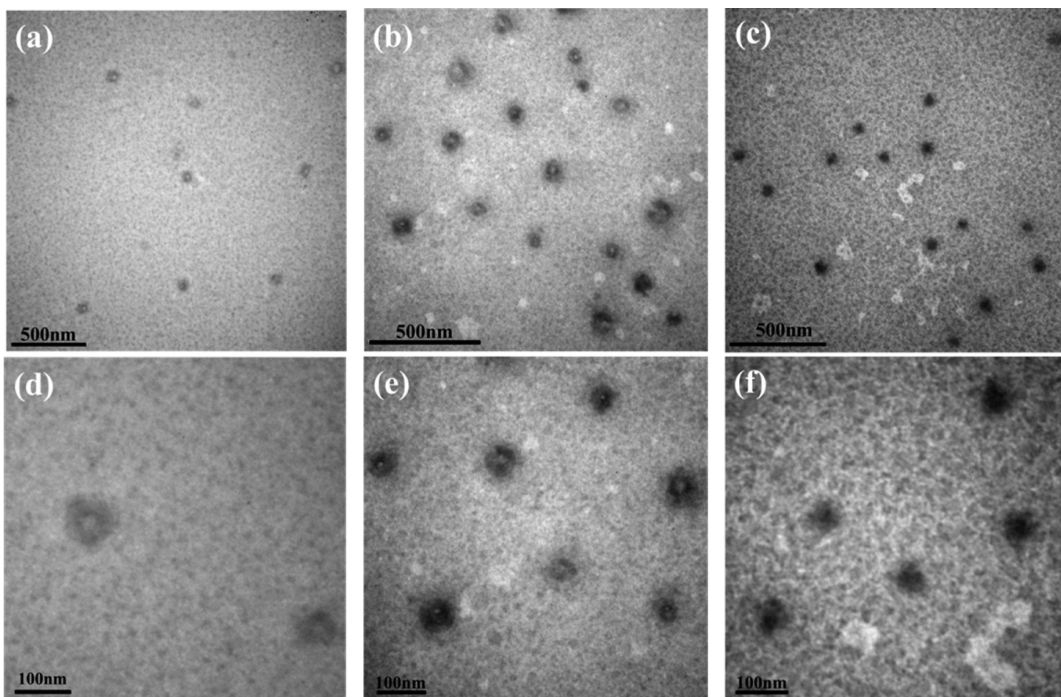
#### Uniform Unimolecular Core–Shell Nanoparticles.

Photo-cross-linkable star-like PCL-*b*-(P(S–N<sub>3</sub>)) diblock copolymers composed of azido groups incorporated into PS shell blocks were then exploited as spherically shaped unimolecular templates to form uniform core–shell polymer nanoparticles by UV exposure. In sharp contrast to the relatively tedious chemical cross-linking widely used for producing polymer nanostructures,<sup>36,38</sup> azido photochemistry allows for photo-cross-linking to occur under mild conditions and requires no additional cross-linking agents. Azido functionality possesses high latent reactivity and easy activation by either heat or UV irradiation.<sup>29,30</sup> In the latter context, the cross-linking density

can be easily controlled by simply varying the intensity of UV irradiation or the irradiation time.

The cross-linking reaction was performed by exposing star-like PCL-*b*-P(S–N<sub>3</sub>) diblock copolymer in chloroform solution to UV irradiation. A dilute solution was used to avoid undesirable intermolecular cross-linking reaction. Successful cross-linking reaction and the formation of polymeric nanoparticles were confirmed by <sup>1</sup>H NMR, FTIR, AFM, and TEM. NMR spectroscopy was utilized to directly monitor the photo-cross-linking process. The intensity corresponding to P(S–N<sub>3</sub>) segment at 4.27, 6.49, and 7.02 ppm labeled as q, o, and n, respectively, in <sup>1</sup>H NMR gradually decreased upon increasing UV exposure time, and completely disappeared at 70 min (SI Figure S5). This implied the formation of nanoparticles with a cross-linked shell (i.e., core–shell nanoparticles).<sup>8</sup> The signals from PCL blocks were also observed in NMR spectra, suggesting the preservation and mobility of PCL inner core in nanoparticles after UV exposure. Uniform core–shell nanoparticles started to form after cross-linking for 20 min as evidenced by AFM measurements (SI Figure S6). Prolonged UV exposure would increase the degree of cross-linking and thus the shell rigidity. Complete disappearance of the peak at 2098 cm<sup>−1</sup> corresponding to azido group in FTIR measurement (SI Figure S7) suggested that the cross-linking of azido groups reached completion at 70 min, which was consistent with NMR analysis (SI Figure S5e). The cross-linked nanoparticles were thus obtained.

Figure 1a shows fully cross-linked nanoparticles (i.e., cross-linked for 70 min) readily visualized by AFM, exhibiting their highly uniform structures upon deposition on Si substrate. A close-up of nanoparticles clearly showed their spherical shape and smooth surface (Figure 1b). The corresponding 3D profile also signified that the deposited nanoparticles on Si substrate were very uniform and of equal height (Figure 1c). Clearly, the spherical shape and monodisperse characteristics of star-like PCL-*b*-P(S–N<sub>3</sub>) templates were retained after their trans-



**Figure 2.** TEM images of core–shell polymeric nanoparticles. (a and d) Light staining where PS shell of nanoparticles was selectively and lightly stained. (b and e) Intermediate staining where PS shell was preferentially and heavily stained. (c and f) Heavy staining where both PCL core and PS shell of nanoparticles were stained.

formation into unimolecular core–shell nanoparticles. The average height  $h_{\text{core–shell, AFM}}$  and diameter  $D_{\text{core–shell, AFM}}$  of fully cross-linked nanoparticles were  $54.1 \pm 2.3$  and  $95 \pm 5.6$  nm, respectively. The discrepancy between  $h_{\text{core–shell, AFM}}$  and  $D_{\text{core–shell, AFM}}$  is due to the AFM tip convolution of nanoparticles, leading to overestimate in lateral size (i.e.,  $D_{\text{core–shell, AFM}} > h_{\text{core–shell, AFM}}$ ). We note that star-like block copolymer template prior to cross-linking would tend to spread out when adsorbed on the substrate because of the chain flexibility. Thus, the average height was less than 10 nm and the template size was not uniform (SI Figure S8). In contrast, a rigid shell was formed after cross-linking which prevented the collapse of nanoparticles. As a result, the height increased significantly upon cross-linking (i.e.,  $54.1 \pm 2.3$  nm) as compared to that of un-cross-linked template (<10 nm).<sup>36,39</sup>

TEM imaging further substantiated that the crafted polymer nanoparticles were spherical and monodisperse (Figure 2). By selectively staining the cross-linked PS shell, core–shell structure of nanoparticles can be clearly revealed by TEM. RuO<sub>4</sub> was employed in the study due to its differential staining capability on PS over PCL. It is crucial to carefully control the staining time to be able to visualize the core–shell structure. The light staining enabled outer PS domains of nanoparticles to be selectively and lightly stained (i.e., appeared dark), so the shell of nanoparticles could be observed under TEM, while the inner PCL blocks appeared transparent (Figure 2a and d). Increasing staining time resulted in intermediate staining. This allowed hollow nanoparticles to be distinctively visualized due to an improved contrast of heavily stained PS shell (Figure 2b and e). Clearly, hollow interiors originating from the unstained PCL core can be seen in almost every nanocapsule (Figure 2a and b). The interface between PCL core and PS shell was rather distinct (Figure 2b and e). Further increase in staining time led to the staining of PCL core as well. Consequently,

entire nanoparticles composed of stained PCL core and PS shell were observed (Figure 2c and f). The average core diameter ( $D_{\text{core, TEM}}$ ) and overall size ( $D_{\text{overall, TEM}}$ ) were  $25.1 \pm 7.9$  and  $58.4 \pm 15.1$  nm, respectively, based on the TEM image analysis at intermediate staining (SI Figure S9a). The comparatively large standard deviation can be attributed to nonuniform staining effect at this staining stage. The image analysis on heavily stained nanoparticles revealed a monodispersed size distribution with  $D_{\text{overall, TEM}}$  of  $50.2 \pm 7.1$  nm (SI Figure S9c). It is worth noting that the core diameter was close to the hydrodynamic diameter  $D_h$  of star-like PCL homopolymer, while the overall size was consistent with  $D_h$  of star-like PCL-*b*-P(S-N<sub>3</sub>) template obtained by DLS (Table 1), signifying that the core size and the shell thickness of nanoparticles were dictated by molecular weights of inner PCL block and outer PS block, respectively. Intriguingly, the diameter determined by TEM correlated well with the height of nanoparticles measured by AFM, suggesting that the fully cross-linked nanoparticles had a rigid shell to maintain the spherical shape without flattening upon the deposition on substrate. The narrow size distribution observed by TEM was also corroborated by AFM measurement. In addition, the DLS measurement on polymeric nanoparticles in chloroform afforded the intensity-average  $D_h$  of  $180.4 \pm 1.8$  nm and a very low polydispersity of 0.11 (SI Figure S10). Compared to  $D_{\text{overall, TEM}}$  determined by TEM, the large  $D_h$  was due possibly to significant swelling of nanoparticles in solution and their surface property.<sup>40</sup> Moreover, during the GPC measurement, a significant decrease in the retention time of star polymer template was observed upon cross-linking (SI Figure S11). We speculate that the rigid cross-linked nanoparticles were unable to rearrange chain conformations to enter small pores or interstices in the GPC columns as the flexible star polymer does. As a result, the smooth nanoparticles were rapidly eluted

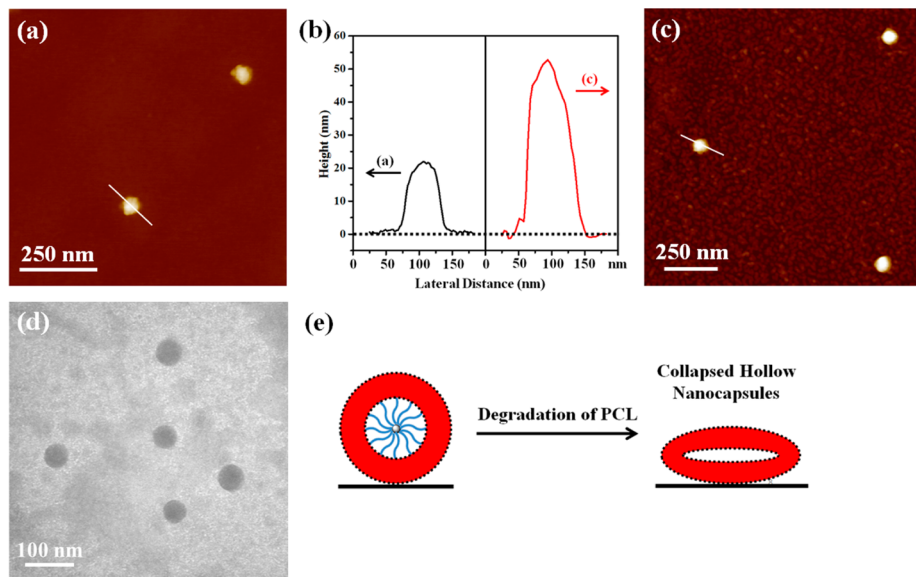


**Figure 3.** Morphologies of hollow polymer nanoparticles. (a) and (c) AFM height images of hollow nanoparticles and core–shell nanoparticles (i.e., prior to degradation of PCL core; fully cross-linked), respectively. (b) Cross-sectional profiles of hollow and core–shell nanoparticles obtained from the corresponding AFM height images in (a) and (c), respectively (i.e., straight lines across nanoparticles in (a) and (c)). (d) TEM image of hollow nanoparticles after staining. (e) Schematic illustration of the transition from core–shell nanocapsule (left) to collapsed hollow nanoparticles (right) on substrate after degradation of PCL blocks.

from the columns with a substantially decreased retention time.<sup>41</sup> On the basis of AFM, TEM, and DLS measurements, star-like PCL-*b*-P(S-N<sub>3</sub>) templates prior to cross-linking exhibited a narrow size distribution.

For comparison, partially cross-linked nanoparticles (i.e., cross-linked for 20 min, SI Figure S6) was also examined by AFM, showing an average height of  $38.6 \pm 2.9$  nm and an average diameter of  $90.7 \pm 9.5$  nm (Figure 1d). Cross-sectional analysis of nanoparticles (Figure 1e) revealed a clear decrease in height (approximately 29%) of partially cross-linked nanoparticles (i.e.,  $38.6 \pm 2.9$  nm, Figure 1d) compared to fully cross-linked nanoparticles (i.e.,  $54.1 \pm 2.3$  nm, Figure 1b), which can be attributed to the fact that nanoparticles with lower cross-linking density are relatively more flexible due to a less rigid shell. As a result, flattening on the substrate would occur for partially cross-linked nanoparticles, and thus a decreased height was observed.<sup>39</sup> The diameter of partially cross-linked nanoparticles (i.e.,  $90.7 \pm 9.5$  nm, Figure 1d) was comparable with fully cross-linked one (i.e.,  $95 \pm 5.6$  nm, Figure 1b) due to the combination of the flattening effect noted above and the lower extent of AFM tip convolution from the reduced height.<sup>42–44</sup> It is worth noting that higher degree of cross-linking led to lower dispersibility and reduced stability of nanoparticles. Fully cross-linked nanoparticles were found to exhibit a good short-term stability, but started to aggregate after long-term storage driven by the minimization of their surface energy as shown in SI Figure S12. Interestingly, partially cross-linked nanoparticles have a good long-term stability and can be redispersed in common organic solvents after drying. Nanoparticles with lower cross-linking density (i.e., partially cross-linked) allowed the penetration of solvent molecules and the swelling of shell, thereby resulting in a good dispersibility. Conversely, a higher degree of cross-linking led to a more rigid structure yet decreased dispersibility of the resulting core–shell nanoparticles.

**Uniform Hollow Polymer Nanoparticles.** To demonstrate in vitro degradability of inner PCL blocks and the

stability of cross-linked nanoparticles, core–shell nanoparticles were hydrolytically degraded under acidic condition, yielding hollow polymer nanoparticles. The success in degradation and formation of hollow nanoparticles was confirmed by a suite of characterization techniques. Complete disappearance of characteristic carbonyl stretching peak at  $1732\text{ cm}^{-1}$  from PCL block in FTIR spectra was indicative of the successful degradation of PCL core (SI Figure S7). A small new peak appeared at  $1716\text{ cm}^{-1}$  after the degradation can be attributed to carbonyl stretching vibration from pendant carboxylic acid groups of the last hydrolyzed PCL unit which remained attached to the inner surface of PS shell.<sup>36</sup> AFM imaging further supported hollow structures of etched nanoparticles (Figure 3). The average height ( $h_{\text{hollow, AFM}}$ ) and diameter ( $D_{\text{hollow, AFM}}$ ) of hollow nanoparticles deposited on Si substrate were approximately  $23.3 \pm 2.5$  and  $66.7 \pm 2.4$  nm, respectively (Figure 3a). The height of nanoparticles decreased about 57% after etching of the PCL core (Figure 3b) from  $54.1 \pm 2.3$  nm ( $h_{\text{core–shell, AFM}}$ , Figure 3c) to  $23.3 \pm 2.5$  nm ( $h_{\text{hollow, AFM}}$ , Figure 3a), suggesting the collapse of hollow nanoparticles on substrate as illustrated in Figure 3e due possibly to the absence of PCL inside support or soft nature of polymer shell for the degraded hollow structure. Notably, in comparison to core–shell nanoparticles, the diameter of hollow nanoparticles measured by AFM was closer to the size evaluated by TEM, which can be ascribed to the lower extent of tip convolution effect as the height of nanoparticles decreased, and thus a higher accuracy in diameter determined by AFM.<sup>42–44</sup> TEM observation showed the formation of remarkably uniform hollow nanoparticles (Figure 3d). The average size obtained from TEM analysis ( $D_{\text{overall, TEM}} = 53.6 \pm 2.6$  nm) was in substantial agreement with the diameter of core–shell nanoparticles prior to core etching ( $D_{\text{overall, TEM}} = 50.2 \pm 7.1$  nm in SI Figure S9c), implying that the structural integrity of nanoparticles was well retained after degradation. No hollow structure can be observed throughout the whole stage of staining; this is not surprising and consistent with AFM characterization, suggesting that hollow nano-

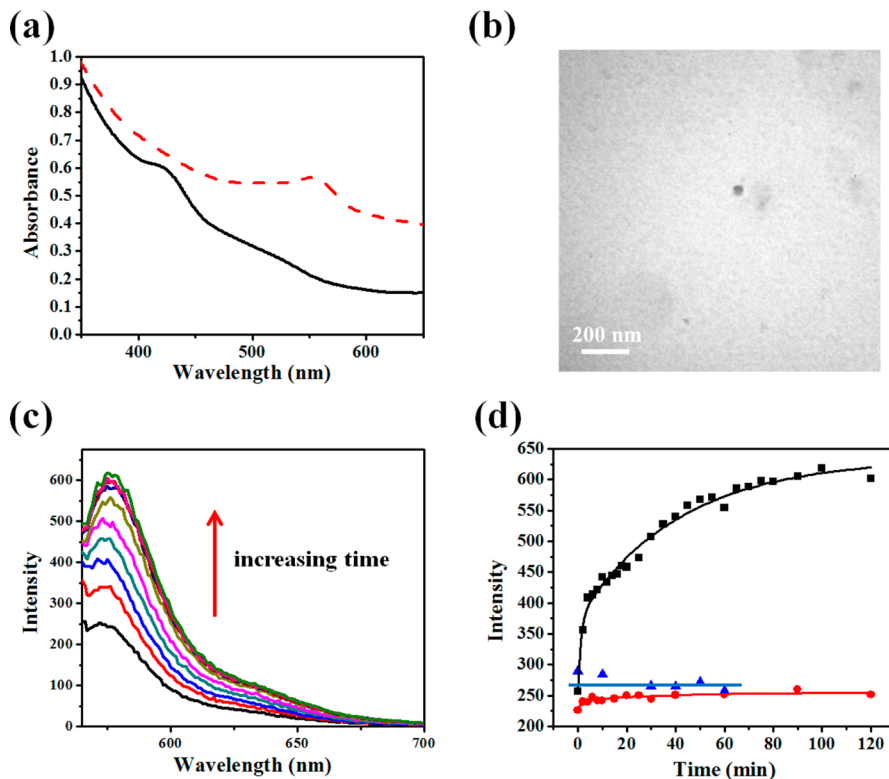


**Figure 4.** Encapsulation and release of dyes. (a) UV-vis spectra of core–shell nanoparticles loaded with two different dyes (i.e., RhB with an absorption maximum of 559 nm (red dash curve) and osmapentalyne with an absorption maximum of 424 nm (black curve)). (b) TEM image of nanoparticles loaded with osmapentalyne. (c) Fluorescence spectra of partially cross-linked nanoparticles loaded with RhB in chloroform. (d) Fluorescence intensity at the emission of 572 nm as a function of time, showing different release rates of RhB from nanoparticles of different cross-linking density in THF and CHCl<sub>3</sub> (i.e., partially cross-linked nanoparticles in CHCl<sub>3</sub> (black squares), fully cross-linked nanoparticles in CHCl<sub>3</sub> (red circles), and partially cross-linked nanoparticles in THF (blue triangles)). The curves are used for guidance.

particles collapsed on the substrate in dry state (Figure 3e). In addition, compared to core–shell nanoparticles, hollow nanoparticles showed slightly longer elution time in the GPC measurement (SI Figure S11), suggesting that the nanoparticles preserved their structure and possibly experienced a small size contraction after degradation. Furthermore, the weight-average molecular weight ( $M_w$ ) determined by SLS decreased approximately  $1.65 \times 10^5$  g/mol from  $4.05 \times 10^5$  g/mol of core–shell nanoparticles upon core etching, which was attributed to the loss of PCL.<sup>41,45</sup> Taken together, the above-mentioned results substantiated the formation of hollow polymer nanoparticles and the maintenance of structural integrity of nanoparticles upon removal of the PCL, which are indicative of the good stability of polymeric nanoparticles.

**Encapsulation and Controlled Release of Fluorescent Probes.** The architecture of nanoparticles plays an important role in encapsulation of a variety of guest molecules, and can thus be employed for controlled release of drugs. In this context, core–shell nanoparticles were exploited as effective nanocarriers by performing encapsulation and release study with dye as a model guest compound. Because of intrinsically spherical architecture of star-like PCL-*b*-P(S-N<sub>3</sub>) templates and the ease of UV-induced cross-linking, we developed a simple and viable route to encapsulating dyes in nanoparticles. Star-like diblock copolymer templates and dyes were first dissolved in solvent. The resulting solution was then exposed to UV irradiation to photo-cross-link the azido-containing PS shell. Extensive purification was subsequently carried out to remove excess dyes outside nanoparticles, thereby yielding dye-

loaded core–shell nanoparticles (denoted nanocarriers; Scheme 1b). It is worth noting that the UV irradiation had negligible effect on the dye stability under the performed experimental conditions.<sup>7,46</sup> Compared to the commonly used nanoprecipitation method,<sup>47</sup> the implemented encapsulation methodology is much simpler. It afforded guest-encapsulated nanocarriers with well-controlled size and narrow size distribution due to monodispersity of star-like PCL-*b*-P(S-N<sub>3</sub>) diblock copolymer template. Two kinds of dyes were selected in the study to demonstrate the versatility of the encapsulation technique. A dye containing Os atom (osmapentalyne,<sup>31</sup> SI Figure S13) was chosen because its inherent metal-containing molecular structure provided dye-loaded nanocarriers the ability for direct TEM imaging.<sup>48</sup> After encapsulation and purification, dye-loaded nanocarriers displayed a characteristic absorption maximum at 424 nm from osmapentalyne,<sup>31</sup> signifying its successful encapsulation (Figure 4a). More importantly, nanocapsule encapsulated with osmapentalyne was directly observed by TEM (Figure 4b). The diameter of nanocarriers was in accordance with that of nanoparticles, reflecting the presence of dyes in both PCL core and PS shell of nanoparticles. On the other hand, when a fluorescent dye is trapped within nanoparticles, the fluorescence self-quenching due to  $\pi-\pi$  interaction would occur due to high local concentration of fluorophore inside.<sup>49</sup> After being released to the surrounding medium, free dyes would manifest a stronger fluorescence upon dilution (i.e., no or much reduced self-quenching). By tracking the increase of fluorescence, the release behavior of guest molecules from nanocarriers can thus

be scrutinized.<sup>7</sup> To this end, Rhodamine B (RhB) was selected as the second fluorescent dye for this study. Star-like PCL-*b*-P(S-N<sub>3</sub>) template was cross-linked for 20 min (i.e., partially cross-linked) together with RhB, and purification was conducted to remove excess RhB. The characteristic absorption peak of RhB at 559 nm from RhB-loaded nanocarriers was clearly evident (Figure 4a), and the emission peak at 572 nm in fluorescence spectra (excitation at 559 nm, Figure 4c) further confirmed the successful encapsulation. A gradual increase in fluorescence intensity was seen when nanocarriers were dissolved in chloroform (CHCl<sub>3</sub>) (Figure 4c), which was due to the release of RhB triggered by the swelling of nanoparticles in chloroform solution. The release kinetics can be obtained by monitoring the fluorescence increase. As shown in Figure 4d, an initial release of RhB was fast and then reached a plateau within 2 h (black squares). The initial burst release was caused by an initial high dilution of RhB outside nanoparticles (i.e., a large concentration gradient of RhB from inside to outside nanocapsule). The release rate was then slowed down due to the decrease in the concentration gradient of RhB across the PS shell of nanoparticles. Quite interestingly, when nanocarriers were dissolved in THF, the RhB release did not obviously occur in light of relatively poor solubility of RhB in THF (blue triangles, Figure 4d), and thus a smaller driving force for dye molecule release. In addition, the effect of shell cross-linking density on release rate was investigated by preparing fully cross-linked nanoparticles loaded with RhB. No obvious dye release in CHCl<sub>3</sub> was found over the same time period using partially cross-linked nanoparticles (red circles, Figure 4d), suggesting a substantially slower release rate. This is due likely to smaller pore sizes in the PS shell because of higher cross-linking density.<sup>38</sup> It is worth noting that we provided a proof-of-principle demonstration that core–shell nanoparticles can act as effective nanocarriers for encapsulating various guest compounds.

The new nanocarriers offer several important and advantageous features, including precise size control via tailoring molecular weights of constituent blocks in star-like diblock copolymers, uniformity, and good stability. Looking ahead, the shell block can be easily replaced with biocompatible cross-linkable polymers to develop new prospective drug nanovehicles. Moreover, PCL blocks situated inside nanoparticles facilitate the loading of drug via hydrophobic interaction,<sup>50–52</sup> and can be readily degraded in vivo with drug release. This will be the subject of future studies.

## SUMMARY

We developed a robust strategy to craft tailororable core–shell and hollow polymer nanoparticles with well-defined architecture, and exploited them as a new type of nanocarrier via the dye encapsulation and release study. The key to our preparative route was the use of photo-cross-linkable core–shell star-like diblock copolymers as templates. Star-like core–shell diblock copolymers were first synthesized by a combination of ring opening polymerization and reversible addition–fragmentation chain transfer polymerization, followed by introducing photo-cross-linking azide moieties on the shell blocks. Interestingly, upon UV irradiation these unimolecular micelles were subsequently transformed into uniform spherical nanoparticles composed of biodegradable inner core blocks and a stable cross-linked shell. The degree of cross-linking can be tailored by varying UV exposure time. The size of nanoparticles is governed by molecular weights of constituent blocks in the

core–shell star-like diblock copolymer template, and the uniformity of nanoparticles was translated from narrow molecular weight distribution of star-like diblock copolymer template. Through the selective removal of the biodegradable inner core, nanoparticles with hollow interiors were produced which retained the structural integrity and stability of as-prepared core–shell nanoparticles. The encapsulation and release of dyes by capitalizing on unimolecular core–shell nanoparticles were also explored as a means to demonstrate the intriguing and effective nanocarrier functionality. We envision that a wide range of well-tailored unimolecular polymer nanoparticles with different compositions and functionalities can be crafted based on this viable templating strategy, dispensing with the need for amphiphilicity as in micelles self-assembled using amphiphilic linear block copolymers. More importantly, drug release may be viably controlled by simply tailoring the cross-linking density of the nanocapsule shell. In addition to spherical star-like diblock copolymers, this strategy can, in principle, be further expanded to utilize more complex polymer compositions and architectures (e.g., bottlebrush-like block copolymer) to create a diversity of truly tailored nanostructures (e.g., polymer nanorods). As such, the development of this new class of polymer nanoparticles with good uniformity and stability, adjustable size, and surface chemistry may present a platform in which to address the size and stability issues widely encountered in current drug nanocarriers.

## ASSOCIATED CONTENT

### Supporting Information

Detailed synthetic procedures and the results on star polymer templates and unimolecular polymer nanoparticles, including NMR, GPC, FT-IR, and UV-vis characterizations; supplemental morphological information on nanoparticles, including AFM, TEM, and DLS characterizations. This material is available free of charge via the Internet at <http://pubs.acs.org>.

## AUTHOR INFORMATION

### Corresponding Author

\*E-mail: zhiquan.lin@mse.gatech.edu.

### Notes

The authors declare no competing financial interest.

## ACKNOWLEDGMENTS

We gratefully acknowledge support from the Air Force Office of Scientific Research (FA9550-13-1-0101 and MURI FA9550-14-1-0037).

## REFERENCES

- (1) Nakayama, M.; Okano, T. *Macromolecules* **2008**, *41*, 504.
- (2) Shimizu, T.; Masuda, M.; Minamikawa, H. *Chem. Rev.* **2005**, *105*, 1401.
- (3) Vriezema, D. M.; Comellas Aragonès, M.; Elemans, J. A.; Cornelissen, J. J.; Rowan, A. E.; Nolte, R. J. *Chem. Rev.* **2005**, *105*, 1445.
- (4) Hayward, R. C.; Pochan, D. J. *Macromolecules* **2010**, *43*, 3577.
- (5) Smith, A. E.; Xu, X.; McCormick, C. L. *Prog. Polym. Sci.* **2010**, *35*, 45.
- (6) Pang, X.; Zhao, L.; Han, W.; Xin, X.; Lin, Z. *Nat. Nanotechnol.* **2013**, *8*, 426.
- (7) Jiang, J.; Qi, B.; Lepage, M.; Zhao, Y. *Macromolecules* **2007**, *40*, 790.
- (8) Nakabayashi, K.; Oya, H.; Mori, H. *Macromolecules* **2012**, *45*, 3197.

- (9) Kakizawa, Y.; Harada, A.; Kataoka, K. *J. Am. Chem. Soc.* **1999**, *121*, 11247.
- (10) Thurmond, K. B.; Kowalewski, T.; Wooley, K. L. *J. Am. Chem. Soc.* **1996**, *118*, 7239.
- (11) He, J.; Tong, X.; Tremblay, L.; Zhao, Y. *Macromolecules* **2009**, *42*, 7267.
- (12) Gao, H.; Matyjaszewski, K. *Macromolecules* **2008**, *41*, 1118.
- (13) Gao, H.; Matyjaszewski, K. *Macromolecules* **2006**, *39*, 4960.
- (14) Gao, H.; Min, K.; Matyjaszewski, K. *Macromol. Chem. Phys.* **2007**, *208*, 1370.
- (15) Fournier, D.; Hoogenboom, R.; Schubert, U. S. *Chem. Soc. Rev.* **2007**, *36*, 1369.
- (16) Altintas, O.; Vogt, A. P.; Barner-Kowollik, C.; Tunca, U. *Polym. Chem.* **2012**, *3*, 34.
- (17) Shi, J.; Votruba, A. R.; Farokhzad, O. C.; Langer, R. *Nano Lett.* **2010**, *10*, 3223.
- (18) Duncan, R. *Nat. Rev. Cancer* **2006**, *6*, 688.
- (19) Torchilin, V. P. *J. Controlled Release* **2001**, *73*, 137.
- (20) Yokoyama, M.; Miyauchi, M.; Yamada, N.; Okano, T.; Sakurai, Y.; Kataoka, K.; Inoue, S. *Cancer Res.* **1990**, *50*, 1693.
- (21) Cao, W.; Zhou, J.; Mann, A.; Wang, Y.; Zhu, L. *Biomacromolecules* **2011**, *12*, 2697.
- (22) Prabaharan, M.; Grailer, J. J.; Pilla, S.; Steeber, D. A.; Gong, S. *Biomaterials* **2009**, *30*, 5757.
- (23) Gu, F.; Zhang, L.; Teply, B. A.; Mann, N.; Wang, A.; Radovic-Moreno, A. F.; Langer, R.; Farokhzad, O. C. *Proc. Natl. Acad. Sci. U. S. A.* **2008**, *105*, 2586.
- (24) Prabaharan, M.; Grailer, J. J.; Pilla, S.; Steeber, D. A.; Gong, S. *Biomaterials* **2009**, *30*, 3009.
- (25) Yang, X.; Grailer, J. J.; Pilla, S.; Steeber, D. A.; Gong, S. *Bioconjugate Chem.* **2010**, *21*, 496.
- (26) Chen, S.; Zhang, X.-Z.; Cheng, S.-X.; Zhuo, R.-X.; Gu, Z.-W. *Biomacromolecules* **2008**, *9*, 2578.
- (27) Perrault, S. D.; Walkey, C.; Jennings, T.; Fischer, H. C.; Chan, W. C. *Nano Lett.* **2009**, *9*, 1909.
- (28) Jiang, W.; Kim, B. Y.; Rutka, J. T.; Chan, W. C. *Nat. Nanotechnol.* **2008**, *3*, 145.
- (29) Bang, J.; Bae, J.; Löwenhielm, P.; Spiessberger, C.; Given-Beck, S. A.; Russell, T. P.; Hawker, C. J. *Adv. Mater.* **2007**, *19*, 4552.
- (30) Yoo, M.; Kim, S.; Lim, J.; Kramer, E. J.; Hawker, C. J.; Kim, B. J.; Bang, J. *Macromolecules* **2010**, *43*, 3570.
- (31) Zhu, C.; Li, S.; Luo, M.; Zhou, X.; Niu, Y.; Lin, M.; Zhu, J.; Cao, Z.; Lu, X.; Wen, T.; Xie, Z.; Schleyer, P. v. R.; Xia, H. *Nat. Chem.* **2013**, *5*, 698.
- (32) Gou, P.-F.; Zhu, W.-P.; Shen, Z.-Q. *Biomacromolecules* **2010**, *11*, 934.
- (33) Gou, P.-F.; Zhu, W.-P.; Xu, N.; Shen, Z.-Q. *J. Polym. Sci., Part A: Polym. Chem.* **2008**, *46*, 6455.
- (34) Moad, G.; Rizzardo, E.; Thang, S. H. *Aust. J. Chem.* **2006**, *59*, 669.
- (35) Moad, G.; Rizzardo, E.; Thang, S. H. *Aust. J. Chem.* **2009**, *62*, 1402.
- (36) Huang, K.; Rzayev, J. *J. Am. Chem. Soc.* **2009**, *131*, 6880.
- (37) Gregory, A.; Stenzel, M. H. *Prog. Polym. Sci.* **2012**, *37*, 38.
- (38) Shanmugananda Murthy, K.; Ma, Q.; Clark, C. G., Jr.; Remsen, E. E.; Wooley, K. L. *Chem. Commun.* **2001**, 773.
- (39) Lemcoff, N. G.; Spurlin, T. A.; Gewirth, A. A.; Zimmerman, S. C.; Beil, J. B.; Elmer, S. L.; Vandeveer, H. G. *J. Am. Chem. Soc.* **2004**, *126*, 11420.
- (40) Ding, Z. Y.; Aklonis, J. J.; Salovey, R. *J. Polym. Sci., Part B: Polym. Phys.* **1991**, *29*, 1035.
- (41) Guo, A.; Liu, G.; Tao, J. *Macromolecules* **1996**, *29*, 2487.
- (42) Allen, M. J.; Hud, N. V.; Balooch, M.; Tench, R. J.; Siekhaus, W. J.; Balhorn, R. *Ultramicroscopy* **1992**, *42*, 1095.
- (43) Villarrubia, J. *J. Res. Natl. Inst. Stand. Technol.* **1997**, *102*, 425.
- (44) Tsukruk, V. V.; Singamaneni, S. *Scanning Probe Microscopy of Soft Matter*; Wiley: New York, 2012.
- (45) Du, J.; Chen, Y. *Macromol. Rapid Commun.* **2005**, *26*, 491.
- (46) Blasco, E.; Schmidt, B. V. K. J.; Barner-Kowollik, C.; Piñol, M.; Oriol, L. *Macromolecules* **2014**, *47*, 3693.
- (47) Farokhzad, O. C.; Cheng, J.; Teply, B. A.; Sherifi, I.; Jon, S.; Kantoff, P. W.; Richie, J. P.; Langer, R. *Proc. Natl. Acad. Sci. U. S. A.* **2006**, *103*, 6315.
- (48) Zhang, K.; Zha, Y.; Peng, B.; Chen, Y.; Tew, G. N. *J. Am. Chem. Soc.* **2013**, *135*, 15994.
- (49) Vogt, T. C. B.; Bechinger, B. *J. Biol. Chem.* **1999**, *274*, 29115.
- (50) Zhang, Y.; Zhuo, R.-x. *Biomaterials* **2005**, *26*, 6736.
- (51) Gaucher, G.; Dufresne, M.-H.; Sant, V. P.; Kang, N.; Maysinger, D.; Leroux, J.-C. *J. Controlled Release* **2005**, *109*, 169.
- (52) Kim, S. Y.; Lee, Y. M. *Biomaterials* **2001**, *22*, 1697.